Characterization of large ferroelectric polarization and high-T_C in sol–gel deposited $PbTiO_3$-based perovskite thin films

To cite this article: Mengqi Ye *et al* 2026 *Chinese Phys. B* **35** 027702

Characterization of large ferroelectric polarization and high-T_C in sol–gel deposited $PbTiO_3$-based perovskite thin films

Mengqi Ye(叶梦琪)[1,2], Zhao Pan(潘昭)[2,†], Weibin Song(宋伟宾)[2], Jin Liu(刘锦)[2], Xubin Ye(叶旭斌)[2], Xin Xiong(熊心)[3], Hui Liu(刘辉)[3], Longlong Fan(樊龙龙)[4], Nianpeng Lu(鲁年鹏)[2], Ruilong Wang(王瑞龙)[1,‡], and Youwen Long(龙有文)[2,5,§]

[1] *Key Laboratory for Intelligent Sensing System and Security of Ministry of Education, School of Physics & School of Microelectrics, Hubei University, Wuhan* 430062, *China*

[2] *Beijing National Laboratory for Condensed Matter Physics, Institute of Physics, Chinese Academy of Sciences, Beijing* 100190, *China*

[3] *School of Physics, University of Science and Technology Beijing, Beijing* 100083, *China*

[4] *Institute of High Energy Physics, Chinese Academy of Sciences, Beijing* 100049, *China*

[5] *Songshan Lake Materials Laboratory, Dongguan* 523808, *China*

(Received 21 May 2025; revised manuscript received 26 June 2025; accepted manuscript online 17 July 2025)

BiMeO$_3$–PbTiO$_3$ (where *Me* represents transition metals) perovskite-type thin films have been widely studied due to their superior ferroelectric properties, including robust ferroelectric polarization and high Curie temperatures. In this study, PbTiO$_3$-based perovskite thin films of xBi(Cu$_{1/2}$Zr$_{1/2}$)O$_3$–$(1-x)$PbTiO$_3$ (xBCZ–$(1-x)$PT) were designed and prepared on Pt(111)/Ti/SiO$_2$/Si substrates using the conventional sol–gel method. The xBCZ–$(1-x)$PT thin films demonstrate remarkable crystallinity, characterized by a perovskite structure and a dense microstructure, which contribute to their high-performance ferroelectric and fatigue properties. Notably, the thin films exhibit large remnant polarization ($2P_r$) values, reaching 98 μC·cm^{-2} and 74 μC·cm^{-2} for the 0.05BCZ–0.95PT and 0.1BCZ–0.9PT compositions, respectively. Furthermore, the thin films also demonstrate a high Curie temperature ($T_C = 510$ °C), as well as favorable fatigue properties and low leakage current, suggesting their potential applicability in ferroelectric devices.

Keywords: ferroelectric thin films, perovskite, sol–gel method, curie temperature

PACS: 77.84.–s, 73.90.+f, 77.84.Cg, 81.20.Fw

DOI: 10.1088/1674-1056/adf0e4 **CSTR:** 32038.14.CPB.adf0e4

1. Introduction

ABO_3 perovskite-type ferroelectric thin films have attracted considerable attention owing to their exceptional ferroelectric properties, exhibiting significant potential for applications in nonvolatile ferroelectric random access memories (FeRAM) and as actuators in microelectromechanical systems (MEMS).[1–3] Driven by the rapid development of ferroelectric materials,[4,5] there is an growing demand for ferroelectric devices capable of operating at elevated temperatures. However, the relatively low Curie temperature (T_C) of conventional ferroelectric materials imposes a significant limitation to their practical applications.[6] Consequently, the exploration of ferroelectric materials exhibiting high T_C remains essential to fulfill the requirements for their practical application and commercialization.

Among the various ferroelectric materials, lead titanate ($PbTiO_3$) and its derivatives have been extensively investigated as representative perovskite ferroelectric compounds.[7,8] $PbTiO_3$ is characterized as a displacive ferroelectric material, exhibiting a tetragonal structure at ambient conditions. It is noted for its high T_C of 490 °C and a significant spontaneous polarization. However, the experimental observation of the substantial spontaneous polarization in bulk $PbTiO_3$ is challenging due to the considerable leakage current inherent in pristine $PbTiO_3$.[9–11] Consequently, numerous high-performance ferroelectric thin films derived from $PbTiO_3$ have been developed, such as the well-known Pb($Zr_{1-x}Ti_x$)O_3 (PZT)[1,2,12] and $BiScO_3$–$PbTiO_3$.[13] In recent decades, significant research attention has been directed towards the BiMeO$_3$–PbTiO$_3$ systems (where *Me* represents mixed cations with an average valence of +3), due to the similar $6s^2$ lone-pair electrons exhibited by Bi^{3+} and Pb^{2+}. The strong hybridization between Bi^{3+}/Pb^{2+} and oxygen is commonly observed in these systems, contributing to their ferroelectric properties.[14] Furthermore, the ferroelectric-active B-site ions (such as Ti and Fe) can exhibit significant hybridization with oxygen, further enhancing ferroelectricity.[13,15–17] It is important to note that the majority of currently reported BiMeO$_3$–PbTiO$_3$ systems incorporate 3d transition metals at the B-site. The low-energy unoccupied states of the transition metals 3d

†Corresponding author. E-mail: zhaopan@iphy.ac.cn
‡Corresponding author. E-mail: wangrl@hubu.edu.cn
§Corresponding author. E-mail: ywlong@iphy.ac.cn

orbitals facilitate hybridization with the O 2p orbitals, thereby enhancing the T_C and ferroelectric polarization. Theoretically, the extensive range of potential B-site cations suggests a significant number of feasible BiMeO$_3$–PbTiO$_3$ systems. Nonetheless, the solubility of many BiMeO$_3$ compounds with PbTiO$_3$ is considerably limited due to the metastable nature of most BiMeO$_3$ end members.[18–20] Consequently, the synthesis of BiMeO$_3$–PbTiO$_3$ compounds typically necessitates a distinct method involving high-pressure and high-temperature conditions.[21–23] It is also noteworthy that the metastable structure of BiMeO$_3$–PbTiO$_3$ systems can also be stabilized in thin film form, attributed to the internal stress exerted by the substrate.[24] High-performance ferroelectric properties were observed in BiMeO$_3$–PbTiO$_3$ thin films, such as the Bi(Zn$_{0.5}$Zr$_{0.5}$)O$_3$–PbTiO$_3$, the Bi(Mg$_{0.5}$Ti$_{0.5}$)O$_3$–PbTiO$_3$, and the Bi(Ni$_{0.5}$Ti$_{0.5}$)O$_3$–PbTiO$_3$ thin films.[24–26] To date, however, only a limited number of BiMeO$_3$–PbTiO$_3$ thin films simultaneously exhibit both substantial ferroelectric polarization and a high T_C. Achieving high T_C while maintaining robust ferroelectric polarization in BiMeO$_3$–PbTiO$_3$ thin films remains a significant challenge.

Based on our prior research which demonstrated that Cu exhibits significant hybridization with oxygen, effectively enhancing ferroelectric polarization and T_C.[27] Furthermore, large piezoelectric response was observed in the Bi(Ni$_{1/2}$Zr$_{1/2}$)O$_3$–PbTiO$_3$ system.[28] It is therefore proposed that Zr may improve the ferroelectric properties. In light of this hypothesis, we designed and deposited a novel perovskite thin films of xBi(Cu$_{1/2}$Zr$_{1/2}$)O$_3$–$(1-x)$PbTiO$_3$ (xBCZ–$(1-x)$PT) using the conventional sol–gel method. As expected, the present thin films demonstrate significant ferroelectric spontaneous polarization, high T_C, and favorable fatigue properties. A comprehensive investigation of the crystal structure and ferroelectric properties was conducted.

2. Experimental details

The xBCZ–$(1-x)$PT ($x = 0.05$ and 0.1) thin films were synthesized on Pt(111)/Ti/SiO$_2$/Si substrate using the conventional sol–gel deposition method. The raw materials employed included lead acetate trihydrate [Pb(COOCH$_3$)$_2$-3H$_2$O], titanium n-butoxide [Ti(OC$_4$H$_9$)$_4$], bismuth nitrate pentahydrate [Bi(NO$_3$)$_3$·5H$_2$O], cupric acetate anhydrous [C$_4$H$_6$CuO$_4$], zirconium nitrate [Zr(NO$_3$)$_4$·5H$_2$O]. These compounds were dissolved in a mixture of 2-methoxyethanol, deionized water, glacial acetic acid, and formamide, and the solution was continuously stirred at room temperature to prepare precursor solutions for the 0.05BCZ–0.95PT and 0.1BCZ–0.9PT compositions. To mitigate the volatilization of Pb and Bi elements, an excess of 10-mol% Pb and 6-mol% Bi was incorporated into the precursor solution. Subsequently, formamide was added to the homogeneous solution to prevent cracking in the thin films. Continuous stirring yielded a uniform BCZ–PT precursor solution with a concentration of 0.2 M. Finally, the precursor solution suitable for spin-coating was obtained by allowing it to age undisturbed for approximately 24 hours.

To enhance the crystallinity of BCZ–PT thin films, a single PbO layer was initially applied via spin-coating, followed by the deposition of BCZ–PT layers, as referenced in studies.[29–32] The PbO seed layer was spin-coated at 5000 rpm for 30 seconds, after which the resulting wet film underwent pyrolysis at 350 °C for 10 minutes. The precursor solution was subjected to identical spin-coating conditions. This process of alternating spin-coating and thermal treatment was systematically repeated for both PbO and BCZ–PT layers, facilitating their deposition onto Pt(111)/Ti/SiO$_2$/Si substrates. The obtained thin films exhibited a thickness of approximately 180 nm. Subsequently, the films were annealed at 700 °C for 30 minutes.

The crystallographic microstructure was examined using the x-ray diffraction (XRD) techniques, utilizing the D2 Phaser (Bruker, Germany and Rigaku, D/max-2000, Cu $K\alpha$ radiation). The inductively coupled plasma optical emission spectroscopy (ICP-OES) was measured by using an inductively coupled plasma atomic emission spectrometer (IRIS Intrepid II, Thermo, America), in order to confirm the chemical composition for the thin films. The cross-sectional morphology of the films was characterized using a field emission scanning electron microscope (FE-SEM, SU8220, Hitachi, Japan). An atomic force microscope (AFM, MultiMode 8, Bruker, Germany) was employed to evaluate the morphology of the as-deposited thin films. The ferroelectric properties, including the polarization–electric field (P–E) hysteresis loop, leakage, and fatigue characteristics, were measured using a ferroelectric analyzer (TF-Analyzer 3000, aix ACCT, Germany).

3. Results and discussion

Figure 1 presents the XRD patterns of the xBCZ–$(1-x)$PT thin films with compositions of $x = 0$, 0.05, and 0.1. All films crystallize in a single-phase perovskite structure (space group $P4mm$), and the peak positions exhibit excellent agreement with the corresponding standard JCPDS card, indicating that the doping of BCZ does not induce a second phase. Note that all the compositions can be indexed as the tetragonal symmetry with space group $P4mm$ by using PowderX software. The related values of $a(b)$ and c axes are 3.914 Å and 4.097 Å, 3.938 Å and 4.016 Å, 3.963 Å and 4.008 Å, for $x = 0$, 0.05, and 0.1, respectively, yielding c/a ratios of 1.047, 1.020, and 1.011, respectively. Consequently, the c/a ratio decreases with increasing BCZ content. This phenomenon has also been observed in numerous other PT-based perovskites.[33–35] The reduction in the c/aratio can be attributed to thermal expansion mismatch and lattice mismatch between the thin films and the

substrates, induced by the internal stress within the BCZ–PT thin films.[36] In order to confirm the chemical composition for the xBCZ–$(1-x)$PT thin films, we performed ICP-OES on the 0.1BCZ–0.9PT sample. Since the substrate contains Ti, which will impact the actual content of Ti during the ICP experiment. Therefore, we just compared the relative content of Pb/Bi/Cu/Zr. The atomic ratio of Pb:Bi:Cu:Zr obtained by ICP-OES is about 1.05:0.0875:0.05:0.05, which agrees well with the ideal atomic ratio of 0.9:0.1:0.05:0.05. The minor discrepancies are mainly attributed to the volatilization of Bi element during the film deposition process.

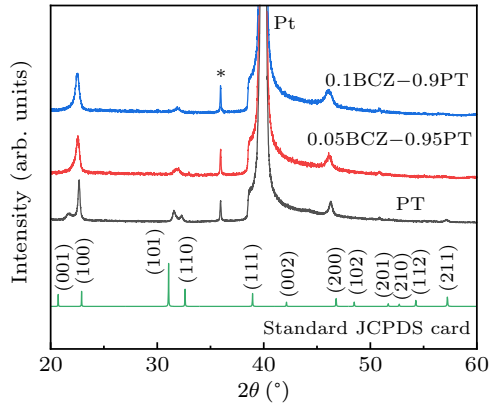

Fig. 1. XRD patterns of the xBCZ–$(1-x)$PT thin films ($x = 0$, 0.05, and 0.1).

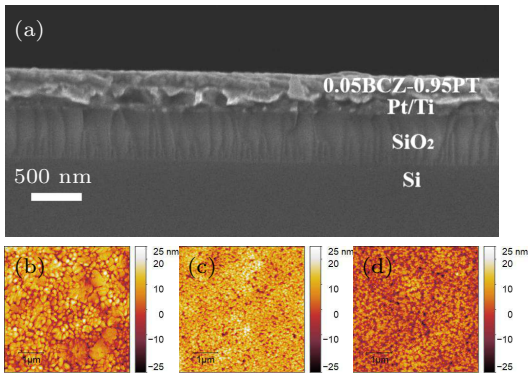

Fig. 2. (a) Cross-sectional SEM image of the 0.05BCZ–0.95PT thin films, AFM images of (b) $PbTiO_3$, (c) 0.05BCZ–0.95PT, and (d) 0.1BCZ–0.9PT thin films, respectively.

Figure 2(a) shows a typical SEM micrograph depicting the cross-sectional view of the 0.05BCZ–0.95PT thin films, clearly delineating the distinct layers of both the substrate and the films. The thickness of the thin films is estimated to be approximately 180 nm. Figures 2(b)–2(d) illustrate the surface morphology of the PT, 0.05BCZ–0.95PT, and 0.1BCZ–0.9PT thin films, respectively. AFM analysis reveals a significant reduction in grain size for both BCZ-doped compositions compared to the undoped PT films. Specifically, the grain sizes range from 100 nm to 300 nm for PT, whereas they decrease to 30 nm–100 nm for both the 0.05BCZ–0.95PT and 0.1BCZ–0.9PT thin films. Furthermore, the smaller grains corresponds to a larger specific surface area, leading to a higher total surface energy in the system. To minimize this energy, the atoms are preferentially filled pores through surface diffusion, thereby promoting the formation of a dense structure. Furthermore, the root mean square (RMS) roughness of the PT thin films is measured at 6.40 nm, while the 0.05BCZ–0.95PT and 0.1BCZ–0.9PT thin films exhibit smoother surfaces, with RMS roughness values of 5.02 nm and 5.80 nm, respectively. Therefore, the 0.05BCZ–0.95PT and 0.1BCZ–0.9PT thin films demonstrate a denser microstructure compared to the PT thin films, which is advantageous for the poling process during the measurement of ferroelectric properties.[33–35]

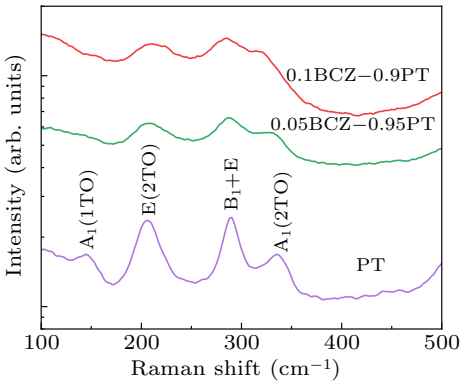

Fig. 3. Raman scattering spectra of the xBCZ–$(1-x)$PT films ($x = 0$, 0.05, and 0.1).

According to the lattice dynamics theory, the vibration of soft modes is intricately linked to ferroelectric properties. In particular, the A_1(1TO) mode, corresponding to the vibration of the TiO_6 octahedron against Pb ions, aligns with the direction of spontaneous polarization (P_S).[37] Consequently, the Raman scattering spectra of xBCZ–$(1-x)$PT ($x = 0$, 0.05, and 0.1) thin films were analyzed (Fig. 3). The spectrum of the PT thin films exhibits four primary peaks, assigned to the A_1(1TO), E(2TO), B_1+E, and A_1(2TO) modes, respectively. The Raman spectra of the xBCZ–$(1-x)$PT thin films with $x = 0.05$ and 0.1 exhibit similar to those of pristine PT thin films, suggesting a tetragonal structure analogous to that of $PbTiO_3$. The relative low Raman intensity of the xBCZ–$(1-x)$PT ($x = 0.05$, and 0.1) thin films could be attributed to the suppressed grain size by the introduction of $Bi(Cu_{1/2}Zr_{1/2})O_3$, as evidenced by the AFM images. The introduction of $Bi(Cu_{1/2}Zr_{1/2})O_3$ reduced the grain size and therefore increased the grain boundary density. The defects at grain boundaries enhances phonon scattering, while stress accumulation at these interfaces modifies local vibrational modes, leading to the attenuation of overall Raman peak intensities. A similar phenomenon was also observed in other $PbTiO_3$-based thin films.[26] Notably, the A_1(1TO) and A_1(2TO) modes shift to lower frequencies as x increases, indicating a softening of these optical modes, which correlates with a reduced c/a ratio. This phenomenon has also been observed in other PT-based ferroelectric systems with a reduced c/a ratio.[38,39] The reduced c/a can be attributed to stress effect induced by the substrate and the size effects. It is

well-established that non-180°domain wall switching is typically associated with significant changes in the c/a ratio.[40,41] A decrease in the c/a ratio can facilitate domain switching, thereby enhancing ferroelectric polarization.[40,41]

Figure 4 illustrates the room-temperature ferroelectric polarization versus electric field $P(E)$ hysteresis loops of xBCZ–$(1-x)$PT thin films ($x = 0$, 0.05, and 0.1). As can be seen in Fig. 4(a), the $P(E)$ loops of PT thin films show significant leakage current. In contrast, the 0.05BCZ–0.95PT thin films exhibit well-saturated $P(E)$ loops with high electrical endurance (Fig. 4(b)), achieving a robust remanent polarization ($2P_r$) value of 98 μC·cm^{-2} at an applied electric field of 600 kV/cm. Similarly, the 0.1BCZ–0.9PT film also yields a substantial $2P_r$ value of 74 μC·cm^{-2} at 350 kV·cm^{-1} (Fig. 4(c)), although a strong leakage current was observed with further increasing the electric field. The coercive field (E_C) values were determined to be 186 kV·cm^{-1} and 138.8 kV·cm^{-1} for the 0.05BCZ–0.95PT and 0.1BCZ–0.9PT thin films, respectively. The elevated E_C observed in the 0.05BCZ–0.95PT thin films may be attributed to several factors, including its small grain sizes, interface characteristics, and a relatively large c/a ratio. It is well established that the c/a ratio significantly influences domain switching,[40,41] with higher electric fields typically required for domain switching in PT-based ferroelectric materials with a large c/a ratio.[40] Consequently, a high electric field applied to the 0.05BCZ–0.95PT thin films is consistent with its large c/a. A large c/a ratio signifies pronounced lattice distortion, stemming from significant off-center displacement of A/B-site cations (P_S displacements).[42] Such distortion necessitates a higher energy barrier for dipole moment reorientation, translating to an increased switching field requirement.[22,43,44] Moreover, the high c/a ratio of the unit cell not only increases the individual dipole moment, but also enhances the dipole moment density per unit volume through the change in the volume of the unit cell, thereby increasing the macroscopic polarization value. Comparatively, the present xBCZ–$(1-x)$PT thin films demonstrate higher P_r values than several other BiMeO$_3$–PbTiO$_3$ thin films, such as 0.1Bi(Zn$_{1/2}$Ti$_{1/2}$)O$_3$–0.9PbTiO$_3$ ($2P_r$ = 56 μC·cm^{-2}), 0.34BiScO$_3$–0.66PbTiO$_3$ ($2P_r$ = 60 μC·cm^{-2}), and 0.25Bi(Ni$_{1/2}$Ti$_{1/2}$)O$_3$–0.75PbTiO$_3$ ($2P_r$ = 81.8 μC·cm^{-2}) thin films.[45–47]

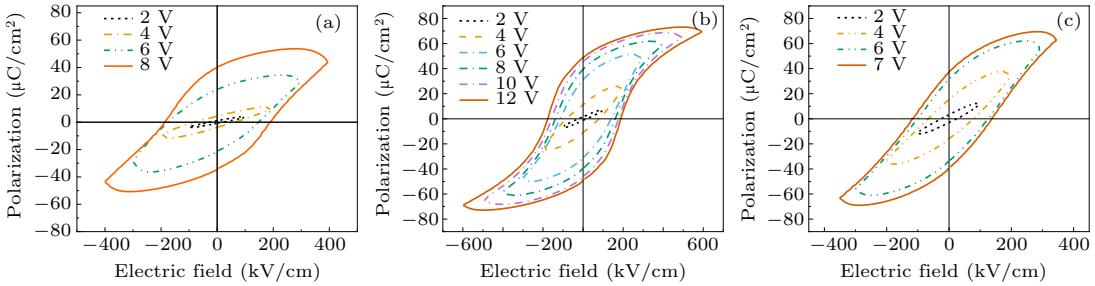

Fig. 4. Ferroelectric hysteresis $P(E)$ loops for the (a) PT, (b) 0.05BCZ–0.95PT, and (c) 0.1BCZ–0.9PT thin films.

Since the xBCZ–$(1-x)$PT thin films exhibit large ferroelectric polarization, its T_C is another one of important parameters for high-performance ferroelectric thin films. The temperature dependence of dielectric constant (ε_r) and loss ($\tan\delta$) for the 0.1BCZ–0.9PT thin films was measured from room temperature up to 500 °C (the maximum temperature for the apparatus) (Figs. 5(a) and 5(b)). The peak around 480 °C corresponds to the ferroelectric to paraelectric phase transition, that is, the T_C. Since the obtained T_C is close to the limiting temperature of the apparatus, we therefore performed the temperature-dependent XRD experiments to further investigate the T_C of the 0.1BCZ–0.9PT thin films, as depicted in Fig. 5(c)). As indicated in the diffraction patterns, the (100) and (200) diffraction peaks exhibit asymmetry at lower temperatures, attributable to the tetragonal structure of the 0.1BCZ–0.9PT thin films. To further investigate the phase transition and accurately determine the T_C, a detailed analysis involving local amplification and multi-peak fitting of the (100) diffraction peak is provided in Fig. 5(d). The observed low-temperature asymmetry is effectively modeled by fitting two peaks corresponding to the (001) and (100) reflections using Voigt functions. Based on these fitting results, the lattice parameters a (b) and c were derived. Upon heating to approximately 510 °C, the (100) peak becomes symmetrical, indicating a transition from the tetragonal to the cubic phase. The temperature-dependent variation of the lattice parameters is comprehensively illustrated in Fig. 5(e). As can be seen, the c-axis parameter decreases while the a-axis parameter increases with increasing temperature, and these parameters converge at approximately $T_C \approx 510$ °C (Fig. 5(e)). It is noted that the slight discrepancy in T_C values between the dielectric measurement and temperature-dependent XRD experiments could be the different accuracy of temperature for the two different apparatuses. Additionally, XRD detection of structural phase transitions requires a discernible level of lattice distortion; a distinct signature typically becomes detectable only upon completion of the phase transition. Consequently, the T_C determined by XRD corresponds more closely to the temperature

at which the phase transition is fully established. In contrast, the dielectric constant exhibits greater sensitivity to local polarization fluctuations. Significant anomalies in the dielectric response, indicative of the onset of the phase transition, can be detected even when the long-range structural transformation is incomplete. Therefore, the T_C measured via dielectric constant is expected to be slightly lower than that measured by the XRD, corresponding to the onset point. This understanding of the measurement methodologies highlights that the present 0.1BCZ–0.9PT thin films simultaneously achieve both large ferroelectric polarization and a high T_C.

In ferroelectric thin films, fatigue properties are crucial determinants of the operational lifespan of ferroelectric devices. Consequently, we investigated the fatigue characteristics of the current BCZ–PT thin films by assessing switchable polarization as a function of increasing electric field cycles. The fatigue behavior of BCZ–PT thin films is depicted in Fig. 6. It is observed that the positive and negative switchable polarization of xBCZ–$(1-x)$PT thin films ($x = 0.05$ and 0.1) progressively decreases with increasing cycle count. After 10^8 cycles, the switchable polarization of 0.05BCZ–0.95PT and 0.1BCZ–0.9PT thin films decreased to approximately 82.3% and 88.3% of their initial values, respectively, which is significantly better than the 64.5% retention observed in pristine $PbTiO_3$.[48] Furthermore, the stable fatigue performance of the present thin films is comparable to that of PZT thin films with Pt electrodes, which exhibit a reduction to 13.3% of the initial switchable polarization after 10^8 cycles.[49] The superior fatigue properties of BCZ–PT thin films may be attributed to their uniform and dense microstructure, as well as their low leakage current.[50]

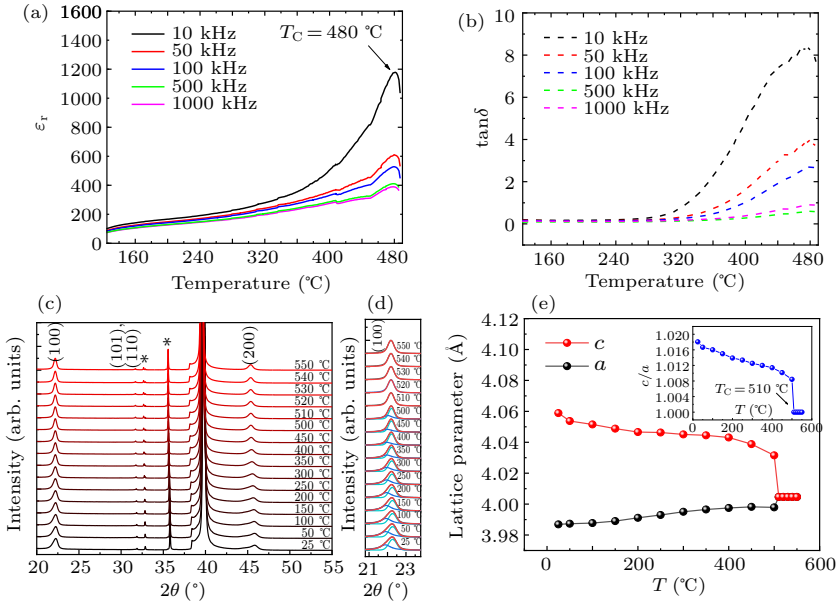

Fig. 5. (a) Dielectric constant (ε_r) and (b) loss ($\tan\delta$) of the 0.1BCZ–0.9PT thin films, (c) temperature dependence of XRD patterns of 0.1BCZ–0.9PT thin films, (d) local amplification of (100) diffraction peaks and multiple peak fitting, and (e) temperature dependence of the lattice parameters of 0.1BCZ–0.9PT thin films. The inset shows the temperature dependence of the c/a ratio.

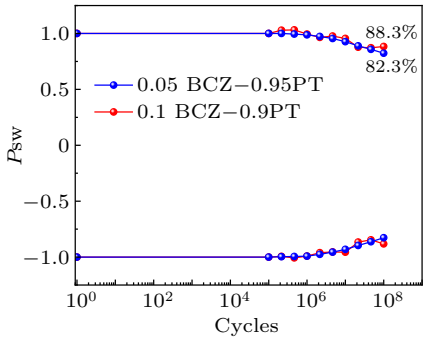

Fig. 6. Normalized switchable polarization *versus* switching cycles for the xBCZ–$(1-x)$PT thin films ($x = 0.05$, and 0.1)

4. Conclusions

In summary, new Bi-based perovskite thin films of $Bi(Cu_{1/2}Zr_{1/2})O_3$–$PbTiO_3$ were deposited on a Pt(111)/Ti/SiO_2/Si substrate utilizing the conventional sol–gel method. The BCZ–PT thin films demonstrate a uniform perovskite structure with a consistent and dense microstructure. Consequently, these films exhibit significant ferroelectric polarization and favorable fatigue characteristics. Furthermore, the BCZ–PT thin films possess a high T_C of 510 °C and exhibit low leakage current. These outstanding comprehensive ferroelectric properties indicate the potential applicability of the thin films in ferroelectric devices.

Acknowledgements

Project supported by the National Key Research and Development Program of China (Grant No. 2021YFA1400300), the National Natural Science Foundation of China (Grant

Nos. 22271309, 12304268, 12261131499, and 11921004), and the China Postdoctoral Science Foundation (Grant No. 2023M743741).

References

[1] Damjanovic D 1998 *Rep. Prog. Phys.* **61** 1267
[2] Scott J F 2007 *Science* **315** 954
[3] Fan L L, Chen J, Wang Q, Deng J X, Yu R Z and Xing X R 2014 *Ceram. Int.* **40** 7723
[4] Wang Z, Yang X, He X, Xue H and Wang X 2023 *Solid State Commun.* **360** 115042
[5] Yao Q, Liu P, Yang F, Zhu Y, Pan Y, Xue H, Mao W and Chu L 2024 *Sci. China Mater.* **67** 3160
[6] Yan Y, Li Z, Li J, Du H, Zhang M, Zhang D and Hao Y 2021 *ACS Appl. Mater. Interfaces* **13** 38517
[7] Samara G A 1971 *Ferroelectrics* **2** 277
[8] Smolenskiĭ G A and Chupis I E 1982 *Sov. Phys. Usp.* **25** 475
[9] Datta K, Margaritescu I, Keen D A and Mihailova B 2018 *Phys. Rev. Lett.* **121** 137602
[10] Song W B, Xi G Q, Pan Z, Liu J, Ye X B, Liu Z H, Wang X, Shan P F, Zhang L X, Lu N P, Fan L L, Qin X M and Long Y W 2024 *Chin. Phys. B* **33** 057701
[11] Cohen R E, Krakauer H 1992 *Ferroelectrics* **136** 65
[12] Wang Y, Zhao H, Zhang L, Chen J and Xing X 2017 *Phys. Chem. Chem. Phys.* **19** 17493
[13] Eitel R E, C A Randall, T R Shrout and S E Park 2002 *Jpn J. Appl. Phys.* **41** 2099
[14] Chen J, Nittala K, Jones J, Hu P and Xing X 2010 *Appl. Phys. Lett.* **96** 252908
[15] Chen J, Sun X, Deng J, Zu Y, Liu Y, Li J and Xing X 2009 *J. Appl. Phys.* **105** 044105
[16] Wu G, Zhou H, Zhou X, Qin N and Bao D 2010 *J. Am. Ceram. Soc.* **93** 925
[17] Zhang S, Eitel R E, Randall C A, Shrout T R and Alberta E F 2005 *Appl. Phys. Lett.* **86** 262904
[18] Suchomel M R, Fogg A M, Allix M, Niu H, Claridge J B and Rosseinsky M J 2006 *Chem. Mater.* **18** 4987
[19] Belik A A, Wuernisha T, Kamiyama T, Mori K, Maie M, Nagai T, Matsui Y and Takayama-Muromachi E 2005 *Chem. Mater.* **18** 133
[20] Belik A A 2012 *J. Solid. State. Chem.* **195** 32
[21] Pan Z, Jiang X, Chen J, Hu L, Yamamoto H, Zhang L, Fan L, Fan X, Li Y, Li G, Ren Y, Lin Z and Azuma M 2018 *Inorg. Chem. Front.* **5** 1277
[22] Pan Z, Chen J, Yu R, Patra L, Ravindran P, Sanson A, Milazzo R, Carnera A, Hu L, Wang L, Yamamoto H, Ren Y, Huang Q, Sakai Y, Nishikubo T, Ogata T, Fan X a, Li Y, Li G, Hojo H, Azuma M and Xing X 2019 *Chem. Mater.* **31** 1296
[23] Pan Z, Chen J, Jiang X, Lin Z, Zhang H, Ren Y, Azuma M and Xing X 2019 *Inorg. Chem. Front.* **6** 1990
[24] Zhang L, Chen J, Zhao H, Fan L, Rong Y, Deng J, Yu R and Xing X 2013 *Dalton Trans.* **42** 585
[25] Xie Z, Peng B, Zhang J, Zhang X, Yue Z and Li L 2015 *Ceram. Int.* **41** S206
[26] Zhang L, Chen J, Zhao H, Fan L, Rong Y, Deng J, Yu R and Xing X 2013 *Appl. Phys. Lett.* **103** 082902
[27] Fan L, Li Q, Zhang L, Shi N, Liu H, Ren Y, Chen J and Xing X 2020 *Inorg. Chem. Front.* **7** 1190
[28] Rong Y, Chen J, Kang H, Liu L, Fang L, Fan L, Pan Z and Xing X 2013 *J. Am. Ceram. Soc.* **96** 1035
[29] Gong W, Li J, Chu X, Gui Z and Li L 2004 *Acta Mater.* **52** 2787
[30] Zhong C, Wang X, Wu Y and Li L 2010 *J. Am. Ceram. Soc.* **93** 3993
[31] Zhong C, Wang X, Guo L and Li L 2015 *Thin Solid Films* **580** 52
[32] Xie Z, Yue Z, Peng B, Zhang J, Zhao C, Zhang X, Ruehl G and Li L 2015 *Appl. Phys. Lett.* **106** 202901
[33] Akdogan E K, Rawn C J, Porter W D, Payzant E A and Safari A 2005 *J. Appl. Phys.* **97** 084305
[34] Jiang B, Peng J L, Bursill L A and Zhong W L 2000 *J. Appl. Phys.* **87** 3462
[35] Ohno T, Suzuki D, Ishikawa K and Suzuki H 2007 *Adv. Powder Technol.* **18** 579
[36] Lee S H, Jang H M, Cho S M and Yi G C 2002 *Appl. Phys. Lett.* **80** 3165
[37] Burns G and Scott B A 1970 *Phys. Rev. Lett.* **25** 167
[38] Burns G and Scott B A 1973 *Phys. Rev. B* **7** 3088
[39] Chen J, Hu P, Sun X, Sun C and Xing X 2007 *Appl. Phys. Lett.* **91** 171907
[40] Leist T, Granzow T, Jo W and Rödel J 2010 *J. Appl. Phys.* **108** 014103
[41] Chen J, Tan X, Jo W and Rödel J 2009 *J. Appl. Phys.* **106** 034109
[42] Chen J, Hu L, Deng J and Xing X 2015 *Chem. Soc. Rev.* **44** 3522
[43] Pan Z, Chen J, Fan L, Liu H, Zhang L, Hu L, Ren Y, Liu L, Fang L, Fan X, Li Y and Xing X 2017 *Inorg. Chem. Front.* **4** 1352
[44] Cohen R E and Krakauer H 1990 *Phys. Rev. B* **42** 6416
[45] Wu G, Zhou H, Qin N and Bao D 2011 *J. Am. Ceram. Soc.* **94** 1675
[46] Zhong C, Wang X, Wen H, Li L, Nan C and Lin Y 2008 *Appl. Phys. Lett.* **92** 222910
[47] Zhong C, Guo L, Wang X and Li L 2011 *J. Am. Ceram. Soc.* **95** 473
[48] Sidorkin A S, Nesterenko L P, Smirnov A L, Smirnov G L, Ryabtsev S V and Sidorkin A A 2008 *Phys. Solid State* **50** 2157
[49] Al-Shareef H N, Kingon A I, Chen X, Bellur K R and Auciello O 2011 *J. Mater. Res.* **9** 2968
[50] Tagantsev A K, Stolichnov I, Colla E L and Setter N 2001 *J. Appl. Phys.* **90** 1387